Photogrammetry for Digital Twinning Industry 4.0 (I4) Systems

Ahmed Alhamadah*, Muntasir Mamun*, Henry Harms*, Mathew Redondo*, Yu-Zheng Lin[†], Jesus Pacheco[‡] Soheil Salehi[†], and Pratik Satam*

*Department of Systems and Industrial Engineering, University of Arizona

†Department of Electrical and Computer Engineering, University of Arizona

‡School of Industrial Engineering, University of Sonora Mexico

Email: {*alhamadah,†yuzhenglin,*muntasir,*henryharms,*mredondo245

,†ssalehi, *pratiksatam}@arizona.edu, ‡jesus.pacheco@unison.mx

Abstract—The onset of Industry 4.0 is rapidly transforming the manufacturing world through the integration of cloud computing, machine learning (ML), artificial intelligence (AI), and universal network connectivity, resulting in performance optimization and increased productivity. Digital Twins (DT) are one such transformational technology that leverages software systems to replicate physical process behavior, and representing it in a digital environment. This paper aims to explore the use of photogrammetry (which is the process of reconstructing physical objects into virtual 3D models using photographs) and 3D Scanning techniques to create accurate visual representation of the 'Physical Process', to interact with the ML/AI based behavior models. To achieve this, we have used a readily available consumer device, the iPhone 15 Pro, which features stereo vision capabilities, to capture the depth of an Industry 4.0 system. By processing these images using 3D scanning tools, we created a raw 3D model for 3D modeling and rendering software for the creation of a DT model. The paper highlights the reliability of this method by measuring the error rate in between the ground truth (measurements done manually using a tape measure) and the final 3D model created using this method. The overall mean error is 4.97% and the overall standard deviation error is 5.54% between the ground truth measurements and their photogrammetry counterparts. The results from this work indicate that photogrammetry using consumer-grade devices can be an efficient and cost-efficient approach to creating DTs for smart manufacturing, while the approaches flexibility allows for iterative improvements of the models over time.

Index Terms—Digital Twin, Photogrammetry, Industry 4.0, Stereo-vision, 3D Reconstruction, Smart Manufacturing

I. INTRODUCTION

As digital technologies advance, Industry 4.0 (I4) represents the next step in manufacturing, development, and education, where the digital and physical worlds intersect, automating cyber-physical systems (CPS), through the use of AI/ML and network connectivity [1], [2]. This adoption of I4 is enabling design and development of Digital Twins, which are virtual environments that digitally mirror the real CPS in all aspects through the use of one or more behavior models [1]–[3].

This work is partly supported by the National Science Foundation (NSF) award number NSF-2335046 and the University of Arizona's Research, Innovation & Impact (RII) award for the "Future Factory".

A DT is a Software System replicating the behavior of one or more physical processes using one or more behavior models, aiming to represent the physical twin's complete lifecycle [1]. DT's aim to combine data-based and physicsbased behavior models, while driven dynamically by real data, allowing for observation and analysis of processes over time [3], [4]. The most advanced twins may connect to real-time data, like an interactive 3D simulation of an active offshore oil platform, while others, sometimes described as digital siblings, enable testing hypothetical situations or performing analysis in an accurate, data-driven environment [2]. This can be particularly useful in manufacturing processes as product design, performance, maintenance, parameters, and assessments can be tested and adjusted in a virtual environment that reacts like the physical system without posing a risk to safety or production [3]. Other industries have also found benefits in using DT environments over simple digital models for the ability to customize environments to specific situations. However, 3D modeling relies on manual use of Computer-Aided Design (CAD) software models that are difficult to acquire, proprietary, and unavailable for heterogeneous systems. For example, for an actual deployment of a factory production line, obtaining a 3D model of each machine is expensive, or not possible, posing a challenge in building a true DT, requiring an efficient framework for the 3D models of each machine combining them with the DT.

Through this paper, we establish a methodology to efficiently build 3D models for digital twinning of Industry 4.0 systems through integration into digital twinning frameworks like the DT4I4-Secure framework proposed by Lin et al. [1] as shown in figure 1, using photogrammetry. The main contributions of this paper:

- The paper presents a methodology to produce 3D models for building DTs, at scale, accurately, and at an inexpensive cost allowing accurate replication of physical systems in a virtual space.
- The paper showcases the use of stereo-vision photogrammetry to create an accurate 3D reconstruction of the

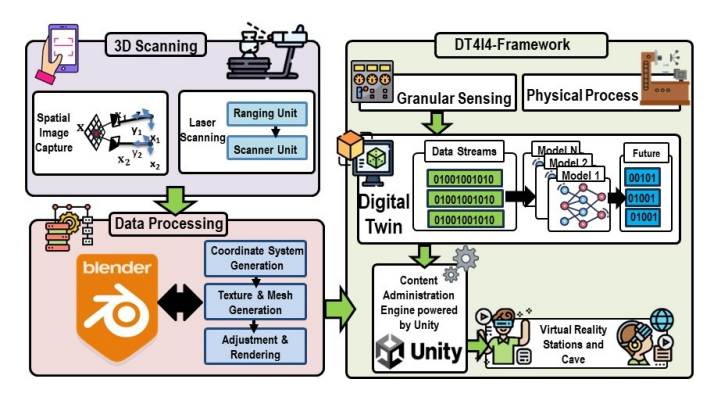


Fig. 1. 3D Scanning and Reconstruction for Industry 4.0 Digital Twin Framework

physical system.

 The paper highlights procedural considerations and error rates in results between the ground truth measurements and the photogrammetry model.

The rest of the paper is organized as follows: In Section II we discuss literature related DT and photogrammetry. In section III we highlight our methodology to use photogrammetry for building accurate 3D models. In section IV we discuss experimental evaluation and results. We finally conclude the paper in section V.

II. LITERATURE REVIEW

This section presents the related work for this paper. The related work is divided into two subsections: Digital Twins and Photogrammetry.

A. Digital Twins (DT)

A DT aims to establish a mirrored connection between the physical and virtual realms, mapping sensor-measured data onto the virtual model. NASA's 2010 technology roadmap draft outlined the utilization of DTs as physical models, updated through sensor feedback to reflect vehicle conditions [5]. Tao et al. propose a DT to be five-dimensional: Physical, Virtual, Connection, Data, and Service. In this five-dimension model, the DT can be applied for several different applications including predictive analysis [6], optimization, and security [7] Lin et al. [1], present a similar five-layered framework to DTs to address Industry 4.0 Security challenges. Similar to Lin's work, DTs find application in system design, optimization, predictive analysis, and education requiring accurate representation and visualization of the physical process to improve the DT's usability [2]. Photogrammetry is an effective method to visualize the physical systems of the DT.

B. Photogrammetry

Photogrammetry is the measurement of an object's distances from multiple photographs of the same object [8]. Photogrammetry through stereo-vision detects the depth between images to generate accurate 3d models of physical objects [9]. While traditionally restricted to specialized scanning equipment, the Internet of Things (IoT) revolution has made photogrammetry

accessible through low end/low cost devices and the combination of digital cameras, LiDAR (Light Detection and Ranging) scanners, and software (combined with artificial intelligence) [10]–[12]. Recent breakthroughs have resulted in improvement in photogrammetry over traditional 3D modeling approaches, allowing photogrammetry to be cheaper through the usage of consumer-grade devices like smartphones and cameras rather than pricey specialized instruments, while allowing greater flexibility and accessibility through IoT connectivity. Furthermore, photogrammetry automates the modeling process, allowing for faster and more accurate development of 3D models, reducing reliance skilled, time-consuming, and manual labor required for traditional approaches [13]. In addition, the ability to continuously refine and update models over time enhances iterative processes, making photogrammetry adaptable to evolving environments and more effective in real-world applications. [13]. Photogrammetry methods such as stereovision photogrammetry enable highly accurate 3D modeling through multiple cameras capturing complex systems from various angles utilizing two horizontal synchronized cameras [14]–[16], with research efforts focused on reduction in measurement uncertainty through using quaternions modeling of the stereo cameras or use of triangulation [17]–[19]. These advancements allow the usage of stereo-vision photogrammetry in manufacturing [14]–[16] and robotics [20]–[22].

III. METHODOLOGY

Our methodology aims to leverage photogrammetry to obtain 3D models to integrate with the DT4I4 Framework as shown in Figure 1. 3D models requiring a reconstruction of images from 2D to 3D, a process that is broken down into multiple stages: Camera Calibration Stage, Image Pair Rectification Stage, and Space Point coordinate calculation Stage. This section describes each of these stages.

A. Camera Calibration

Camera calibration estimates intrinsic and extrinsic parameters to map 2D image points to 3D world points [23], [24]. Intrinsic parameters define internal camera characteristics like focal length and optical center, while extrinsic parameters describe the camera's position and orientation [23], [25]. By capturing images of a known geometry, calibration enables a rigid transformation from world to camera coordinates, crucial for 3D reconstruction [24], [26], [27]. This process shown in Figure 2 enables accurate camera calibration allowing accurate reconstruction of the scene's geometry. [26], [27].

These parameters are configured using a planar pattern-based camera calibration algorithm [28]. A point on a 2D plane is represented by $k_s = [u\,v]$. A point on a 3D plane is represented by $K_s = [X_w, Y_w, Z_w]$. To scale these, 1 is added to the last element of each of them. k = [u, v, 1] and $K = [X_w, Y_w, Z_w, 1]$. Through the pinhole phenomena, we gain the relationship between both 3D points and their 2D projection [28]. Equations (1) and (2) explain that relationship.

$$ck_s = b \begin{bmatrix} N & e \end{bmatrix} K_s \tag{1}$$

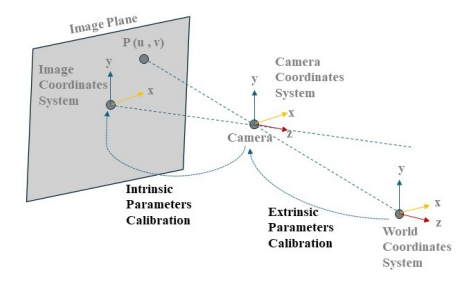


Fig. 2. Camera Calibration Process

$$c \begin{bmatrix} u \\ v \\ 1 \end{bmatrix} = \begin{bmatrix} \alpha_u & \gamma & u_0 \\ 0 & \alpha_v & v_0 \\ 0 & 0 & 1 \end{bmatrix} \begin{bmatrix} N & e \end{bmatrix} \begin{bmatrix} X_w \\ Y_w \\ Z_w \\ 1 \end{bmatrix}$$
 (2)

We denoted the scaling factor as c, the pixel focus as $[\alpha_u,\alpha_v]$, which are the scaling factors of images in 2D plane axes, the distortion parameters as γ , and the principle point coordinates as $[u_0,v_0]$. The camera's extrinsic parameters include the rotation matrix N and the translation vector e. The relative position of both stereo cameras is determined by calculating the associated external parameters as shown in equation (3):

$$\begin{cases} N_{RL} = N_r N_l^{-1} \\ e_{RL} = e_r - N_r N_l^{-1} e_l \end{cases}$$
 (3)

The variables $[N_l,e_l]$ and $[N_r,e_r]$ represent the rotation matrices and translation vectors of the stereo cameras on the right and left, respectively, with respect to a specific world coordinate system. Similarly, we denote the rotation matrix and translation vector between the two cameras as N_{RL} and e_{RL} respectively.

B. Image Pair Rectification

Image pair rectification aligns points in left and right images on the same plane through a transmission-projection transformation [29]. We compute the transformation matrices and apply them to the images using bilinear interpolation [30], which linearly interpolates both image variables. The projection points must satisfy the following fundamental equation:

$$\mathbf{p}_{r}^{T}\mathbf{b}_{r}^{-T}[\mathbf{e}_{RL}]_{x}\mathbf{N}_{RL}\mathbf{b}_{l}^{T}\mathbf{p}_{l} = 0$$

$$\tag{4}$$

We denote the left and right projection points of a point by \mathbf{p}_l and \mathbf{p}_N respectively. We also denote the intrinsic parameters of the right and left cameras by \mathbf{b}_r and \mathbf{b}_l . Similarly, we denote the antisymmetric matrix by $[\mathbf{e}_{RL}]_x$ which we derived from the translation vector \mathbf{e}_{RL} .

C. Space Point Coordinates Calculation

We determine the coordinates of the points in space using the triangle measuring method, which we defined using equation (5):

$$\begin{cases} X_w(x,y) = \frac{G \times O \times (x_l - u_o l)}{\alpha_{ul} \times (x_l - x_r)} \\ Y_w(x,y) = \frac{G \times O \times (y_l - v_o l)}{\alpha_{vl} \times (x_l - x_r)} \\ Z_w(x,y) = \frac{G \times O}{x_l - x_r} \end{cases}$$
 (5)

We denote the variables as follows: the coordinates of spatial points as (X_w, Y_w, Z_w) ; the pixel focal length of the left camera is represented as $[\alpha_{ul}, \alpha_{vl}]$; the optical center distance between both cameras as G; the pixel focal length of the camera is represented as O; the principal point coordinate of the left camera as (u_{0l}, v_{0l}) ; and (x_l, y_l) and (x_r, y_r) are the rectified coordinates of the left-right projection points m_l and m_r , respectively.

Consequently, by using a triangulation algorithm, we can fit the spatial point cloud, which is points in space that represent the 3D shape, to obtain a curved surface after we computed it using Equation (5) completing the 3-D reconstruction.

IV. EXPERIMENTAL EVALUATIONS

A. Experiment Setup

The section provides an overview of the setup we used to execute this experiment.

- 1) UArizona Future Factory: The UArizona Future Factory is an Industry 4.0 system featuring four SMC Corporation's Smart Innovation Factory (SIF) 400 stations, developer stations, and data collection/attacker stations. It simulates an automated smart factory using machine-to-machine connectivity for production, assembly, logistics, and management. The SIF-400 consists of four interconnected modular stations on a conveyor belt: SIF 401: Stores and transports containers on RFID-tagged pallets, SIF 402: Fills containers with solid materials, SIF 405: Attaches caps to containers and SIF 407: Labels and dispatches containers. The experiments presented in this paper focus on modeling of the SIF405: Capping Station.
- 2) Stereo-Vision Cameras iPhone 15 Pro: The iPhone 15 Pro, with three cameras and a lidar scanner powered by the A17 Pro chip, is a cost-effective platform for photogrammetry. Its 6-core CPU, 6-core GPU, and 16-core neural engine enable real-time data processing [31]. It is the only iPhone

TABLE I CAMERA SPECIFICATIONS

Camera	Specification
	24 mm
48MP Main	f/1.78
	Sensor-Shift OIS
	24MP/48MP Photos
	13 mm
12MP Ultra Wide	f/2.2
	120° FOV
	100 Focus Pixel

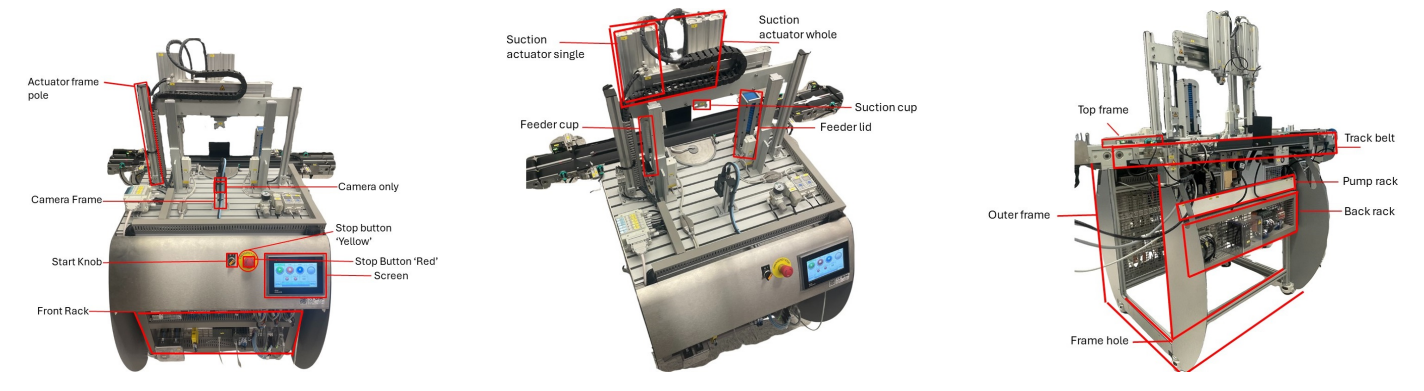


Fig. 3. A. Labeled snapshot for the front section, B. Labeled snapshot for the top section, C. Labeled snapshot for the back section







Fig. 4. A. Reconstructed 3D model of the front section, B. Reconstructed 3D model of the top section, C. Reconstructed 3D model of the back section

capable of using stereo-vision technology for capturing photos and videos, making it ideal for fast and accurate 3D model generation [31].

The specifications of each camera are highlighted in Table I. For this work, we used stereo images and lidar scans from an iPhone 15 Pro stitched together with AI-assisted tools like Polycam to create 3D models in Blender.

3) Software for model creation: Polycam stitches stereo images with lidar scans using AI, lidar, and triangulation algorithms to create accurate 3D point clouds. This makes Polycam a valuable tool for creating digital twins on an iPhone. Blender, an open-source tool, optimizes raw 3D scans by generating meshes, performing retopology, and applying textures via UV unwrapping, producing refined and efficient 3D models.

B. Experiments

To create a visual digital twin of the SIF 405, we followed four steps. First, we recorded ground truth measurements of the testbed using a tape measure. Next, we captured 3D images with the iPhone 15 Pro's stereo-vision technology. Then, we processed these images in Polycam, using the "full" setting for detailed texture maps and "Raw" for a single texture file, and applied object masking to handle environmental factors. Finally, we imported the Polycam output into Blender,

adjusting the 3D model's position, scale, and orientation to precisely compare measurements with the ground truth.

1) Experiment 1: Measuring the accuracy of the front section: In our first experiment, we measured the length (L), width (W), and height (H) of key components from the front view of the SIF 405: Capping Station as baseline data. Lidar scans imported real-world measurements into Blender, while photogrammetry scans required alignment for scale, rotation, and origin. Blender was used to match photogrammetry scans with lidar data, enabling accurate 3D model measurements for comparison with the baseline. Figure 3A, 4A show a snapshot and modeled front view of the capping station respectively for comparison.

We compared the scanned dimensions to the actual measurements and found error rates detailed in Table II. Some dimensions, especially small details like I/O buttons, had error rates of 10-20% due to limitations in the iPhone's imaging resolution, which can obscure thin details. Despite this, most scanned dimensions were accurate within 5-10%, with some, such as the width of the front rack, height of the actuator frame pole, and length of the start switch, showing errors under 1%.

2) Experiment 2: Measuring the accuracy of the top section: In our second experiment, we measured the length (L), width (W), and height (H) of major components from a side view of the testbed station. Figure 3B, 4B show the snapshot and modeled side view for comparison. We compared photogrammetry data with ground truth measurements and

TABLE II FRONT SECTION MEASUREMENTS

Objects	L			W			Н		
	Actual	iPhone 15 Pro	Error	Actual	iPhone 15 Pro	Error	Actual	iPhone 15 Pro	Error
Actuator Frame Pole	1.125	1.193	6.04%	1.125	1.184	5.24%	16.84375	16.687	0.93%
Camera Frame	1.125	1.012	10.04%	1.125	1.069	4.98%	6.375	6.318	0.89%
Camera Only	1.75	1.706	2.51%	2.0625	1.943	5.79%	3.5	3.389	3.17%
Start Knob (Red Circle)	1.125	1.395	24.00%	1.63	1.766	8.34%	1.625	1.451	10.71%
Stop Button (Yellow Circle)	2.6875	2.895	7.72%	0	0	0%	2.75	2.934	6.69%
Start Switch (O/1)	1.125	1.133	0.71%	1.07	1.042	2.62%	1.75	1.795	2.57%
Screen	7.875	7.556	4.05%	0.25	0.248	0.80%	5.5	5.21	5.27%
Front Rack	29.155	28.462	2.38%	2.34375	2.336	0.33%	20.65625	20.338	1.54%

TABLE III
TOP SECTION MEASUREMENTS

Objects	L			W			Н		
	Actual	iPhone 15 Pro	Error	Actual	iPhone 15 Pro	Error	Actual	iPhone 15 Pro	Error
Suction Actuator Whole	12.15625	12.056	0.82%	1.21875	1.311	7.57%	9.125	9.072	0.58%
Suction Actuator Single	4.25	4.306	1.32%	1.21875	1.311	7.57%	9.125	9.072	0.58%
Feeder Lid	2.25	2.332	3.64%	2.09375	2.506	19.69%	9.59375	9.588	0.06%
Feeder Cup	2.125	2.254	6.07%	1.5	1.456	2.93%	10.375	9.593	7.54%
Suction Cups	3.4375	3.46	0.65%	1.375	1.468	6.76%	2.125	2.186	2.87%

TABLE IV
BACK SECTION MEASUREMENTS

Objects	L				W		H		
	Actual	iPhone 15 Pro	Error	Actual	iPhone 15 Pro	Error	Actual	iPhone 15 Pro	Error
Top Frame	28.5	28.303	0.69%	20	20.003	0.02%	2.47	1.905	22.87%
Frame Hole	31.5	31.151	1.11%	21.97	18.728	14.76%	28.75	28.452	1.04%
Track Belt	48.375	45.73	5.47%	5.25	5.216	0.65%	2.31	2.048	11.34%
Pump Rack (White)	29.875	29.471	1.35%	2.78125	2.282	17.95%	2.34375	2.313	1.31%
Back Rack	29.375	28.929	1.52%	2.34375	2.276	2.89%	8.34375	8.188	1.87%
Outer Frame	31.75	31.364	1.22%	41.47	37.501	9.57%	34.25	32.294	5.71%

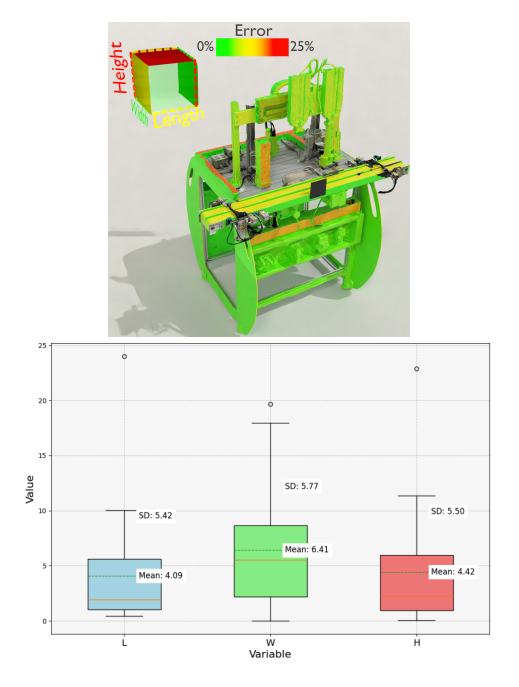


Fig. 5. A. Error heatmap, B. Mean average and standard deviation distribution

error rates are detailed in III. We focused on large compo-

nents, such as the outer frame, interior hole, and track belt. Most dimensions were within 1-6% error, but measurements in the W direction had higher errors (10-18%), likely due to environmental conditions and alignment issues. Some H measurements, like those for the top frame and track belt, also had high error rates due to background complexity affecting the photogrammetry algorithm.

3) Experiment 3: Measuring the accuracy of the back section: In the final experiment, we measured the length (L), width (W), and height (H) of major components from a top view before imaging. Figure 3C, 4C shows the snapshot and the modeled back view for comparison. Table IV details actual and scanned measurements with error rates. Most errors were under 8%, with many below 1%. Some W measurements had higher errors due to obscured geometry, including a 19% error for the feeder lid, indicating that the photogrammetry camera's shape affects accuracy in tight spaces. We highlighted the error distribution and focus in the heat map figure 5 showing where the errors mostly occurred in the 3D model as we discussed in the experiments. We also provide the overall mean and standard deviation values of the error in figure 5.

V. CONCLUSION

In conclusion, this experiment highlighted the importance of accurately replicating physical systems in virtual spaces for the benefits provided by Digital Twins in Industry 4.0. We presented a method for creating visualizations for Smart Manufacturing Digital Twins using consumer-grade hardware and software, specifically the iPhone 15 Pro, IoT, networked scanning, and 3D processing tools. The method achieved reliable 3D models with an average error of 4.97% and a standard deviation of 5.54%. While factors like object placement, background complexity, and tight spaces affected accuracy, the method still produced 90-95% accurate dimensions, proving effective for reflecting physical processes in a cyber-physical system.

REFERENCES

- [1] Y.-Z. Lin, S. Shao, M. H. Rahman, M. Shafae, and P. Satam, "Dt4i4-secure: Digital twin framework for industry 4.0 systems security," in 2023 IEEE 14th Annual Ubiquitous Computing, Electronics & Mobile Communication Conference (UEMCON). IEEE, 2023, pp. 0200–0209.
- [2] A. Rasheed, O. San, and T. Kvamsdal, "Digital twin: Values, challenges and enablers from a modeling perspective," *IEEE access*, vol. 8, pp. 21980–22012, 2020.
- [3] L. Wright and S. Davidson, "How to tell the difference between a model and a digital twin," Advanced Modeling and Simulation in Engineering Sciences, vol. 7, pp. 1–13, 2020.
- [4] Q. Qi, F. Tao, T. Hu, N. Anwer, A. Liu, Y. Wei, L. Wang, and A. Y. Nee, "Enabling technologies and tools for digital twin," *Journal of Manufacturing Systems*, vol. 58, pp. 3–21, 2021.
- [5] E. Glaessgen and D. Stargel, "The digital twin paradigm for future nasa and us air force vehicles," in 53rd AIAA/ASME/ASCE/AHS/ASC structures, structural dynamics and materials conference 20th AIAA/ASME/AHS adaptive structures conference 14th AIAA, 2012, p. 1818.
- [6] M. Shafto, M. Conroy, R. Doyle, E. Glaessgen, C. Kemp, J. LeMoigne, and L. Wang, "Modeling, simulation, information technology & processing roadmap," *National Aeronautics and Space Administration*, vol. 32, no. 2012, pp. 1–38, 2012.
- [7] D. Holmes, M. Papathanasaki, L. Maglaras, M. A. Ferrag, S. Nepal, and H. Janicke, "Digital twins and cyber security-solution or challenge?" in 2021 6th South-East Europe Design Automation, Computer Engineering, Computer Networks and Social Media Conference (SEEDA-CECNSM). IEEE, 2021, pp. 1–8.
- [8] M. Magnani and M. Douglass, "Photogrammetry and stereophotogrammetry," in SAS Encyclopedia of Archaeological Sciences. Hoboken: Wiley-Blackwell, 2018.
- [9] M. Magnani, M. Douglass, W. Schroder, J. Reeves, and D. R. Braun, "The digital revolution to come: Photogrammetry in archaeological practice," *American Antiquity*, vol. 85, no. 4, pp. 737–760, 2020.
- [10] R. C. Anderson, "Photogrammetry: the pros and cons for archaeology," World Archaeology, vol. 14, no. 2, pp. 200–205, 1982.
- [11] A. Fussell, "Terrestrial photogrammetry in archaeology," World Archaeology, vol. 14, no. 2, pp. 157–172, 1982.
- [12] S. A. Turpin, R. P. Watson, S. Dennett, and H. Muessig, "Stereophotogrammetric documentation of exposed archaeological features," *Journal of field archaeology*, vol. 6, no. 3, pp. 329–337, 1979.
- [13] A. Morichon, G. Dannhoff, L. Barantin, C. Destrieux, and I. L. Maldonado, "Doing more with less: Realistic stereoscopic three-dimensional anatomical modeling from smartphone photogrammetry," *Anatomical Sciences Education*, vol. 17, no. 4, pp. 864–877, 2024.
- [14] Z. Yin and J. Xiong, "Stereovision measurement of layer geometry in wire and arc additive manufacturing with various stereo matching algorithms," *Journal of Manufacturing Processes*, vol. 56, pp. 428–438, 2020.
- [15] Z. Wang, R. Liu, T. Sparks, H. Liu, and F. Liou, "Stereo vision based hybrid manufacturing process for precision metal parts," *Precision Engineering*, vol. 42, pp. 1–5, 2015.
- [16] D. Samper, J. Santolaria, F. J. Brosed, and J. J. Aguilar, "A stereovision system to automate the manufacture of a semitrailer chassis," *The International Journal of Advanced Manufacturing Technology*, vol. 67, pp. 2283–2292, 2013.

- [17] F. Lavecchia, M. Guerra, and L. Galantucci, "The influence of software algorithms on photogrammetric micro-feature measurement's uncertainty," *The International Journal of Advanced Manufacturing Technol*ogy, vol. 93, pp. 3991–4005, 2017.
- [18] International Organization for Standardization (ISO), Uncertainty of Measurement—Part 3: Guide to the Expression of Uncertainty in Measurement (GUM: 1995). ISO/IEC Guide 98-3:2008, 2008.
- [19] X. Chen, J. Lin, Y. Sun, H. Ma, and J. Zhu, "Analytical solution of uncertainty with the gum method for a dynamic stereo vision measurement system," *Optics Express*, vol. 29, no. 6, pp. 8967–8984, 2021.
- [20] J. Wang, B. Tao, Z. Gong, S. Yu, and Z. Yin, "A mobile robotic measurement system for large-scale complex components based on optical scanning and visual tracking," *Robotics and Computer-Integrated Manufacturing*, vol. 67, p. 102010, 2021.
- [21] J. T. C. Tan and T. Arai, "Triple stereo vision system for safety monitoring of human-robot collaboration in cellular manufacturing," in 2011 IEEE International Symposium on Assembly and Manufacturing (ISAM). IEEE, 2011, pp. 1–6.
- [22] J.-K. Oh and C.-H. Lee, "Development of a stereo vision system for industrial robots," in 2007 International Conference on Control, Automation and Systems. IEEE, 2007, pp. 659–663.
- [23] Z. Zhang, "Camera calibration," in *Multiple View Geometry in Computer Vision*, R. Hartley and A. Zisserman, Eds. Cambridge University Press, 2004, ch. 2, pp. 101–140.
- [24] MathWorks, "Camera calibration," accessed: 2024-05-25. [Online]. Available: https://www.mathworks.com/help/vision/ug/camera-calibration.html
- [25] J. Heikkila and O. Silvén, "A four-step camera calibration procedure with implicit image correction," in *Proceedings of IEEE computer* society conference on computer vision and pattern recognition. IEEE, 1997, pp. 1106–1112.
- [26] J. Y. Bouguet, "Camera calibration toolbox for matlab," *Computational Vision at the California Institute of Technology*, n.d.
- [27] M. Berger, Geometry I. Springer-Verlag, 2009, translated from the 1977 French original by M. Cole and S. Levy, fourth printing of the 1987 English translation.
- [28] Z. Zhang, "A flexible new technique for camera calibration," *IEEE Transactions on pattern analysis and machine intelligence*, vol. 22, no. 11, pp. 1330–1334, 2000.
- [29] A. Fusiello, E. Trucco, and A. Verri, "A compact algorithm for rectification of stereo pairs," *Machine vision and applications*, vol. 12, pp. 16–22, 2000.
- [30] R. C. Gonzalez and R. E. Woods, *Digital Image Processing*, 4th ed. Pearson Prentice Hall, 2008.
- [31] W. contributors, "Apple a17," https://en.wikipedia.org/wiki/Apple_A17, 2023, accessed: 2024-09-07.